

PCCP

Physical Chemistry Chemical Physics

Accepted Manuscript

This article can be cited before page numbers have been issued, to do this please use: I. R. Ariyaratna, *Phys. Chem. Chem. Phys.*, 2025, DOI: 10.1039/D5CP02454D.



This is an Accepted Manuscript, which has been through the Royal Society of Chemistry peer review process and has been accepted for publication.

Accepted Manuscripts are published online shortly after acceptance, before technical editing, formatting and proof reading. Using this free service, authors can make their results available to the community, in citable form, before we publish the edited article. We will replace this Accepted Manuscript with the edited and formatted Advance Article as soon as it is available.

You can find more information about Accepted Manuscripts in the [Information for Authors](#).

Please note that technical editing may introduce minor changes to the text and/or graphics, which may alter content. The journal's standard [Terms & Conditions](#) and the [Ethical guidelines](#) still apply. In no event shall the Royal Society of Chemistry be held responsible for any errors or omissions in this Accepted Manuscript or any consequences arising from the use of any information it contains.

Ground and Excited State Properties of ThBe and AcBe

Isuru R. Ariyarathna

Theoretical Division, Los Alamos National Laboratory, Los Alamos, NM 87545, United States

E-mail: isuru@lanl.gov

ABSTRACT

In this work, the ground and excited states of ThBe and AcBe were investigated by performing high-level multireference and single-reference coupled-cluster quantum chemical calculations with large correlation consistent basis sets. Full potential energy curves (PECs), chemical bonding patterns, energetics, spectroscopic parameters (T_e , r_e , ω_e , and $\omega_e x_e$), and spin-orbit effects of 13 and 8 electronic states of ThBe and AcBe, respectively, are reported. The ground electronic states of ThBe and AcBe are single-reference $1^3\Sigma^- (1\sigma^2 2\sigma^2 1\pi^2)$ and $1^2\Pi (1\sigma^2 2\sigma^2 1\pi^1)$, respectively, and originate from their corresponding ground state fragments. The chemical bonding of ThBe ($1^3\Sigma^-$) and AcBe ($1^2\Pi$) are π -dative in character that are formed by d-electron transfers from Th/Ac to the empty $2p_x$ and $2p_y$ of the Be atom. The electron populations of the f-orbitals of both ThBe ($1^3\Sigma^-$) and AcBe ($1^2\Pi$) are minor which exhibit their “transition-metal-like” natures. The estimated bond energies of the spin-orbit ground states of ThBe ($1^3\Sigma^-_{0+}$) and AcBe ($1^2\Pi_{1/2}$) are 12.79 and 11.02 kcal/mol, respectively. Finally, the bond energy of ThBe was used to estimate its heat of formation ΔH_f° (298 K) of 869.61 ± 6 kJ/mol.



I. INTRODUCTION

Even though modern quantum chemical methods are capable of providing rather accurate predictions for a variety of chemical systems, many are challenged by the complexity of transition metal, lanthanide, and actinide based diatomic species. Such small complexes often bear a series of closely-lying low-energy electronic states spawning from the near-degenerate d- and f-orbitals. Hence the resolution of these states often requires the adaptation of high-level *ab initio* wave function theories. Furthermore, accounting for the spin-orbit coupling effects and relativistic effects could be crucial for gaining accurate theoretical predictions on their chemophysical properties, especially in the absence of experimental data.¹⁻³

On many occasions, the wave functions of diatomic species are composed of multi electron configurations (multireference) (especially in excited states and stretched regions of the potential energy surfaces) and hence cannot be described properly by single reference techniques, which encourages the use of multireference quantum calculations for their characterizations. Nevertheless, such calculations are computationally expensive and require a great deal of technical skills and knowledge to overcome associated convergence issues. Furthermore, multireference calculations often require manipulation of the active spaces for proper treatment of the static and dynamic electron correlations and would otherwise provide unreasonable predictions. The multireference configuration interaction singles and doubles (MRCI) level of theory is ideal for the investigation of highly correlated species. Furthermore, the application of the Davidson correction (MRCI+Q) to MRCI energies can provide further accurate predictions especially on correlated metal diatomic species.⁴⁻⁸ This is indeed due to the approximate quadruple-like substitution effect of the MRCI+Q level. Additionally, in the cases of minor spin-orbit coupling, the single-reference electronic states can be described very accurately by coupled-cluster theories. Therefore, these levels are often utilized for carrying out systematic quantum chemical studies of molecules.

Investigations of chemical bonding and excited state properties of actinide based species are of great interest to the progression of the field of nuclear energy.⁹⁻¹² Especially, fundamental electronic properties of diatomic molecules can be used to produce models to understand their macroscale properties¹³, finetune desired chemical reactions in nuclear fuel cycles^{14, 15}, and to help remediate current nuclear waste issues^{14, 16, 17}. Hence, recently a series of high-level theoretical attempts have been made to predict and understand ground and excited properties of actinide-based diatomic species¹⁸⁻²⁰ with a special attention to the p-block elements and H atom bonded U and Th diatomic systems.²¹⁻²⁹ Surprisingly, such studies of Th + Be and U + Be reactions are almost nonexistent. This could be due to the lack of experimental interest on them as a result of the toxicity



of beryllium³⁰ and low stabilities of such complexes due to the closed-shell electron configuration of the ground state of Be.³¹ Indeed, the only available study on UBe was reported very recently by Peterson and Dixon research groups, which provided insight on its very weak bond.¹³ However, usually Be is one of the most chemically versatile s-block elements that readily participates in a variety of chemical reactions producing ionic, covalent, and dative-type chemical bonding, hence, its reaction with Th is curious case to study.³²⁻³⁷ Furthermore, reports on the chemical bonding of actinium-based species is less available in the literature due to its transition metal like properties and high cost due to low abundance of Ac in earth's crust.³⁸ Overall, to date, ThBe and AcBe species are not yet studied experimentally or theoretically, hence this work was conducted to understand their bonding, excited states, and energetics.

In the present work, the MRCI, MRCI+Q, coupled-cluster singles, doubles, and perturbative triples [CCSD(T)], and coupled-cluster singles, doubles, triples, and perturbative quadruples [i.e., CCSDT(Q)] theories with correlation consistent basis sets were utilized to study full PECs, chemical bonding patterns, energetics, spectroscopic constants of 13 and 8 electronic states of ThBe and AcBe. 23 and 8 spin-orbit states of ThBe and AcBe are also studied. Furthermore, the core electron correlation effects and the complete basis set effects on their properties are also reported.

II. COMPUTATIONAL DETAILS

All internally contracted MRCI (or MRCISD)³⁹⁻⁴¹ and CCSD(T)⁴² calculations were performed with MOLPRO 2023.2⁴³⁻⁴⁵ software suite. The C_{2v} symmetry was used for calculations. All calculations were performed with the triple-zeta and quadruple-zeta quality correlation consistent basis sets. Specifically, for the calculations of ThBe, the following five basis set combinations were used: (1) cc-pVTZ⁴⁶ of Be and cc-pVTZ-PP⁴⁷ of Th [hereafter, TZ], (2) cc-pVQZ⁴⁶ of Be and cc-pVQZ-PP⁴⁷ of Th [hereafter, QZ], (3) cc-pVQZ-DK⁴⁶ of Be and cc-pVQZ-DK3⁴⁸ of Th [hereafter, QZ-A], (4) cc-pVTZ⁴⁶ of Be and cc-pwCVTZ-PP⁴⁷ of Th [hereafter, TZ-C], (5) cc-pVQZ⁴⁶ of Be and cc-pwCVQZ-PP⁴⁷ of Th [hereafter, QZ-C]. The inner 60 electrons of the Th atom ($1s^2 2s^2 2p^6 3s^2 3p^6 3d^{10} 4s^2 4p^6 4d^{10} 4f^{14}$) were replaced by the Stuttgart-Köln energy-consistent full relativistic pseudopotential (ECP60)⁴⁹ in all calculations except for when using the (3)rd all electron set that performed on third-order DKH Hamiltonian. For AcBe (1) cc-pVTZ-DK⁴⁶ of Be and cc-pVTZ-DK3⁴⁸ of Ac [hereafter, TZ], (2) cc-pVQZ-DK⁴⁶ of Be and cc-pVQZ-DK3⁴⁸ of Ac [hereafter, QZ], (3) cc-pVTZ-DK⁴⁶ of Be and cc-pwCVTZ-DK3⁴⁸ of Ac [hereafter, TZ-C], and (4) cc-pVQZ-DK⁴⁶ of Be and cc-pwCVQZ-DK3⁴⁸ of Ac [hereafter, QZ-C] basis set combinations were used with the third-order DKH Hamiltonian. The complete active space self-consistent field⁵⁰⁻⁵³ (CASSCF) reference wave functions were provided for MRCI calculations. The



CASSCF wave functions of ThBe and AcBe were produced by including 6 and 5 electrons in 13 active orbitals, respectively. At bond dissociation limits of ThBe and AcBe, these 13 active orbitals are purely the 2s and three 2p atomic orbitals of Be and the 7s, five 6d, and three 7p atomic orbitals of Th and Ac. At the C_{2v} symmetry, these orbitals are $6a_1$ ($6d_{z^2}$, $6d_{x^2-y^2}$, 7s, and $7p_z$ of Th and 2s and $2p_z$ of Be), $3b_1$ ($6d_{xz}$ and $7p_x$ of Th and $2p_x$ of Be), $3b_2$ ($6d_{yz}$ and $7p_y$ of Th and $2p_y$ of Be), and $1a_2$ ($6d_{xy}$ of Th).

First, at the QZ-MRCI level, full PECs of $\text{Th}(^3\text{F}; 6d^27s^2)+\text{Be}(^1\text{S}; 2s^2)$, $\text{Th}(^3\text{P}; 6d^27s^2)+\text{Be}(^1\text{S}; 2s^2)$, $\text{Th}(^1\text{D}; 6d^27s^2)+\text{Be}(^1\text{S}; 2s^2)$, and $\text{Th}(^5\text{F}; 6d^37s^1)+\text{Be}(^1\text{S}; 2s^2)$ were calculated. In the AcBe case, $\text{Ac}(^2\text{D}; 6d^17s^2)+\text{Be}(^1\text{S}; 2s^2)$, $\text{Ac}(^2\text{P}^0; 7s^27p^1)+\text{Be}(^1\text{S}; 2s^2)$, $\text{Ac}(^4\text{F}; 6d^27s^1)+\text{Be}(^1\text{S}; 2s^2)$, $\text{Ac}(^4\text{F}^0; 6d^17s^17p^1)+\text{Be}(^1\text{S}; 2s^2)$, $\text{Ac}(^4\text{P}; 6d^27s^1)+\text{Be}(^1\text{S}; 2s^2)$, and $\text{Ac}(^2\text{D}^0; 6d^17s^17p^1)+\text{Be}(^1\text{S}; 2s^2)$ reactions were investigated to compute QZ-MRCI PECs of its most stable states. At the MRCI level, all active electrons (6 of ThBe and 5 of AcBe) and $6s^26p^6$ electrons of Th/Ac were correlated to the virtual orbitals. Specifically, in MRCI calculations of ThBe the $5s^25p^65d^{10}$ electrons of Th and $1s^2$ of Be are frozen whereas all remaining inner electrons of Th are represented by ECP60. In AcBe MRCI calculations all $1s^22s^22p^63s^23p^63d^{10}4s^24p^64d^{10}4f^{14}5s^25p^65d^{10}$ electrons of Ac and $1s^2$ of Be are frozen. The Davidson correction (MRCI+Q)⁵⁴ implemented in MOLPRO was applied to evaluate the approximate quadruple substitution effect. At the QZ-MRCI level, the dipole moment curves of ThBe were obtained. Implementing the same electron correlation effects and active spaces, the spin-orbit coupling calculations were performed at QZ-MRCI+Q level (hereafter, QZ-MRCI+Q-SO). For spin-orbit calculations spin-orbit pseudopotential operator (for ThBe) and Breit-Pauli Hamiltonian (for AcBe) were used. The MRCI spin-orbit matrix elements were provided for MRCI+Q spin-orbit calculations and the MRCI energies were replaced with MRCI+Q energies. More details on the spin-orbit calculations are discussed in the main text of the paper.

All coupled-cluster calculations were built on restricted open-shell Hartree Fock (ROHF) wave functions. The PECs of single-reference $1^3\Sigma^-$ and $1^3\Pi$ of ThBe and $1^2\Pi$ of AcBe, were also calculated around their equilibrium bond ranges at the QZ-CCSD(T) level. At the CCSD(T) level, all valence electrons (which also includes $6s^26p^6$) of Th/Ac were correlated. The TZ-C-CCSD(T) and QZ-C-CCSD(T) equilibrium PECs of ThBe ($1^3\Sigma^-$ and $1^3\Pi$) and AcBe ($1^2\Pi$) were also calculated by further correlating the outer-core $5d^{10}$ electrons of Th/Ac. The TZ-C-CCSD(T) and QZ-C-CCSD(T) PECs and their ROHF PECs were employed to obtain PECs at the complete basis set (CBS) limit [hereafter, CBS-C-CCSD(T)]. Here, ROHF absolute energies and dynamic electron correlations were extrapolated separately and added together. Specifically, for the ROHF energy extrapolation, a scheme presented by Pansini et al. (see, Ref. 55, equation 9) was used. The CBS extrapolation of the dynamic electron



correlation was carried out under the unified-single-parameter-extrapolation method introduced by the same research group (see, Ref. 56 equation 2). The effects of the higher-order T(Q) electron correlations were also addressed by performing TZ-CCSDT(Q) calculations. All valence electron correlations were considered. The MRCC^{57, 58} code linked to MOLPRO was used for these coupled-cluster calculations. The $\delta T(Q)$ [i.e., $\delta T(Q) = E_{TZ-CCSDT(Q)} - E_{TZ-CCSD(T)}$] effect was added to the CBS-C-CCSD(T) values to calculate more accurate CBS-C-CCSD(T)+ $\delta T(Q)$ bond energies of ThBe and AcBe. The coupled-cluster dipole moment of ThBe was calculated under the finite-field method embedded in MOLPRO by applying a field of 0.0125 a.u.

The MRCI, MRCI+Q, CCSD(T), C-CCSD(T), and CBS-C-CCSD(T) PECs of ThBe and AcBe were used to introduce their spectroscopic parameters. The natural bond orbital (NBO) equilibrium electron charges and populations of ThBe and AcBe were investigated using the NBO7^{59, 60} code linked to MOLPRO.

III. RESULTS AND DISCUSSION

IIIA. ThBe

The full PECs are useful to gain a thorough understanding of the origins, avoided crossings, positions of energy minima, and stabilities of diatomic molecules. Furthermore, such PECs are vital for producing their radiative models. Hence, as the first step of this work, the PECs of ThBe were studied considering Th(³F; 6d²7s²)+Be(¹S; 2s²), Th(³P; 6d²7s²)+Be(¹S; 2s²), Th(¹D; 6d²7s²)+Be(¹S; 2s²), and Th(⁵F; 6d³7s¹)+Be(¹S; 2s²) reactions.³¹ These reaction combinations produce ³[Σ^- , Π , Δ , Φ], ³[Σ^- , Π], ¹[Σ^+ , Π , Δ], and ⁵[Σ^- , Π , Δ , Φ] molecular states for ThBe, respectively. The QZ-MRCI+Q PECs of these electronic states of ThBe are given as a function of Th...Be distance in the Figure 1. All 13 PECs originating from the aforementioned reactions are attractive in nature. The ground state fragments [i.e., Th(³F)+Be(¹S)] produce the 1³ Σ^- ground electronic state of ThBe with an approximate bond energy of 20 kcal/mol. The second excited state of ThBe (i.e., 1³ Π) also resulting from the ground state fragments (Figure 1) and lies ~7 kcal/mol above the ground state. Around 2.5-2.7 Å, 1³ Π and 2³ Π PECs display slight shoulders which could be due to avoided crossings. Furthermore, the shoulders of the PECs of these two states could be caused by a higher energy ³ Π state. The third lowest energy fragments [i.e., Th(¹D; 6d²7s²)+Be(¹S; 2s²)] gives rise to the first excited state of ThBe which is a 1¹ Δ . Both third and fourth excited states of ThBe (i.e., 1⁵ Δ and 1⁵ Σ^-) are products of the Th(⁵F)+Be(¹S) reaction. Next, we see 1¹ Σ^+ , 1³ Φ , 2³ Π , 1¹ Π , and 1⁵ Φ states of ThBe lying as close as 2 kcal/mol to each other highlighting the complexity of the excited state electronic spectrum of this



system. It should be noted that the PECs of $1^3\Delta$ and $2^3\Sigma^-$ of Figure 1 are not complete due to the observed convergence issues at the MRCI level.

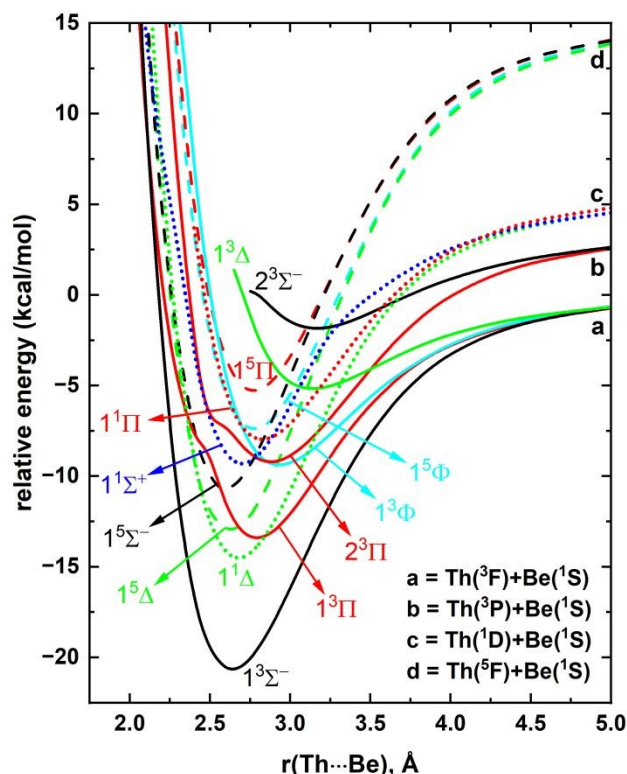
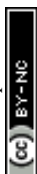


Figure 1. QZ-MRCI+Q PECs of ThBe as a function of Th...Be distance [$r(\text{Th}\cdots\text{Be})$, Å]. The relative energies are referenced to the dissociation limit of $\text{Th}(^3\text{F}) + \text{Be}(^1\text{S})$, which is set to 0 kcal/mol. The Σ^+ , Σ^- , Π , Δ , and Φ states are shown in blue, black, red, green, and cyan, respectively. The dashed, solid, and dotted PECs correspond to the quintet, triplet, and singlet spin electronic states, respectively.

The dominant equilibrium electronic configurations of the 13 studied electronic states of ThBe are given in Table 1. The CASSCF state average molecular orbitals produced by including these 13 states of ThBe at 2.65 Å are illustrated in Figure 2. The 1σ molecular orbital of ThBe carries 69% of 2s of Be and 25% of 7s and 6% of $6d_{z^2}$ of Th. The 2σ is composed of 66% of 7s and 16% $6d_{z^2}$ of Th and 18% of 2s of Be. The 3σ elegantly captures the hybridization of the $2p_z$ of Be and $6d_{z^2}$ of Th (Figure 2). The $1\pi_x$ (or $1\pi_y$) bonding molecular orbital of ThBe is a mixture of the $6d_{xz}$ (or $6d_{yz}$) of Th (78%) and $2p_x$ (or $2p_y$) of Be (22%). The $1\delta_{x^2-y^2}$ and $1\delta_{xy}$ non-bonding orbitals ThBe represent the pure $6d_{x^2-y^2}$ and $6d_{xy}$ atomic orbitals of the Th atom, respectively.



The ground electronic state of ThBe ($1^3\Sigma^-$) carries the dominantly single-reference $1\sigma^2 2\sigma^2 1\pi^2$ electron configuration. Based on the shapes of the $1\pi_x$ and $1\pi_y$ we can recognize two π -dative d-electron transfers from Th to $2p_x$ and $2p_y$ of the Be atom for ThBe ($1^3\Sigma^-$). The ThBe ($1^3\Sigma^-$) ground state is closely related to the ground electronic state of ThB ($1^4\Sigma^-$).⁶¹ Specifically, the addition on an electron to the vacant 3σ of ThBe ($1^3\Sigma^-$) creates the single-reference electron configuration of ThB ($1^4\Sigma^-$; $1\sigma^2 2\sigma^2 3\sigma^1 1\pi^2$).⁶¹ According to the NBO analysis performed at the QZ-ROHF, the ThBe ($1^3\Sigma^-$) bears the Th[$6d^{1.98} 7s^{1.91} 5f^{0.19} 7p^{0.17}$]Be[$2s^{1.65} 2p^{0.09}$] electron population. The atomic electron affinity of Th atom is 0.61 eV^{21, 62} while Be⁻ is not stable.³⁸ Therefore, we can expect Th ^{δ^-} Be ^{δ^+} charge localization for ThBe. On the other hand, the electronegativities of Th and Be atoms are 1.3 and 1.57, respectively, hence it is also natural to expect Th ^{δ^+} Be ^{δ^-} polarization for the ThBe molecule.⁶³ However, according to our NBO analysis the ground electronic state of ThBe ($1^3\Sigma^-$) carries a charge distribution of Th^{-0.26}Be^{+0.26} which aligns with Th ^{δ^-} Be ^{δ^+} polarization prediction based on the electron affinities. The less ionic-like nature of this bond could be the reason for its relatively low bond energy (i.e., ~20 kcal/mol, Figure 1). The first excited state of ThBe is a multireference $1^1\Delta$ with $1\sigma^2 2\sigma^2 1\pi_x^2 \pm 1\sigma^2 2\sigma^2 1\pi_y^2$ electron configuration (Table 1). An electron promotion from $1\pi_x$ or $1\pi_y$ of ThBe ($1^3\Sigma^-$) to its empty 3σ creates the single-reference second excited electronic state of ThBe (i.e., $1^3\Pi$; $1\sigma^2 2\sigma^2 3\sigma^1 1\pi^1$). The $1^5\Delta$ is the first electronic state of ThBe to populate non-bonding 1δ orbitals, which is also the most stable quintet-spin state of the ThBe molecule. Among all studied states, the $1^5\Sigma^-$ of ThBe carries the highest bond-order (i.e., 1.5) with populated bonding 3σ sigma and $1\pi_x$ and $1\pi_y$ orbitals (i.e., $1\sigma^2 2\sigma^2 3\sigma^1 1\pi^2$). The higher bond-order of this state translates to its bond distance which is the shortest among all states of ThBe studied (Table 1 and Figures 1 and 2). Considering the equilibrium electron configurations and the molecular orbital profiles, the valence bond Lewis (vbL) of the first five electronic states of ThBe were introduced and given in Figure 3. All proceeding electronic states of ThBe are multireference in character except for the $1^3\Delta$ (Table 1).

The QZ-MRCI dipole moment curves of the 13 states of ThBe as a function of Th...Be distance are illustrated in Figure 4. The dipole moment of the ground $1^3\Sigma^-$ of ThBe at its r_e is -0.90 D. This value is in excellent agreement with the finite-field approach [at QZ-C-CCSD(T)] predicted dipole moment which is -0.91. Among all states the largest dipole moment (at equilibrium distances) was observed for the $1^5\Sigma^-$ which is -2.99 D. The permitted lowest energy transitions of ThBe ($1^3\Sigma^-$) are $1^3\Sigma^- \leftrightarrow 1^3\Pi$ and $1^3\Sigma^- \leftrightarrow 2^3\Pi$ (Figure 1). The transition dipole moment (TDM) curves of $1^3\Sigma^- \leftrightarrow 1^3\Pi$ and $1^3\Sigma^- \leftrightarrow 2^3\Pi$ as well as the $1^3\Pi \leftrightarrow 2^3\Pi$ are given in ESI Figure S1. The minimum of the TDM curve of $1^3\Sigma^- \leftrightarrow 1^3\Pi$ coincide with the r_e of $1^3\Sigma^-$. The $1^3\Sigma^- \leftrightarrow 2^3\Pi$ TDM minimum (-0.08 D) was observed around ~3.8 Å.



The transition between $1^3\Pi \leftrightarrow 2^3\Pi$ is also significant with a minimum at 3.4 Å of its TDM curve (ESI Figure S1).

Table 1. Dominant electronic configurations at equilibrium distances of the studied 13 electronic states of ThBe. ^a

State ^b	Coefficient ^c	Configuration ^d
$1^3\Sigma^-$	0.87	$1\sigma^2 2\sigma^2 1\pi_x 1\pi_y$
$1^1\Delta$	0.58	$1\sigma^2 2\sigma^2 1\pi_x^2$
	-0.58	$1\sigma^2 2\sigma^2 1\pi_y^2$
$1^3\Pi$	0.85	$1\sigma^2 2\sigma^2 3\sigma 1\pi_x$
$1^5\Delta$	0.93	$1\sigma^2 2\sigma 1\pi_x 1\pi_y 1\delta_{xy}$
$1^5\Sigma^-$	0.90	$1\sigma^2 2\sigma 3\sigma 1\pi_x 1\pi_y$
$1^3\Phi$	0.60	$1\sigma^2 2\sigma^2 1\pi_y 1\delta_{xy}$
	0.60	$1\sigma^2 2\sigma^2 1\pi_x (1\delta_{x^2-y^2})$
$1^1\Sigma^+$	0.57	$1\sigma^2 2\sigma^2 1\pi_x^2$
	0.57	$1\sigma^2 2\sigma^2 1\pi_y^2$
$2^3\Pi$	0.55	$1\sigma^2 2\sigma^2 1\pi_x (1\delta_{x^2-y^2})$
	-0.55	$1\sigma^2 2\sigma^2 1\pi_y 1\delta_{xy}$
$1^1\Pi$	0.59	$1\sigma^2 2\sigma^2 3\sigma 1\pi_x$
	-0.59	$1\sigma^2 2\sigma^2 3\sigma 1\pi_x$
$1^5\Phi$	0.66	$1\sigma^2 2\sigma 3\sigma 1\pi_y 1\delta_{xy}$
	0.66	$1\sigma^2 2\sigma 3\sigma 1\pi_x (1\delta_{x^2-y^2})$
$1^5\Pi$	-0.64	$1\sigma^2 2\sigma 3\sigma 1\pi_y 1\delta_{xy}$
	0.64	$1\sigma^2 2\sigma 3\sigma 1\pi_x (1\delta_{x^2-y^2})$
$1^3\Delta$	0.92	$1\sigma^2 2\sigma^2 3\sigma (1\delta_{x^2-y^2})$
$2^3\Sigma^-$	0.71	$1\sigma^2 2\sigma^2 (1\delta_{x^2-y^2}) 1\delta_{xy}$
	0.34	$1\sigma^2 2\sigma 3\sigma (1\delta_{x^2-y^2}) 1\delta_{xy}$

^a The coefficients and electron configurations were collected under state-average QZ-CASSCF that includes all studied 13 electronic states of ThBe. ^b The B_1 components of Π and Φ states and A_1 of the Δ states under C_{2v} symmetry are listed. ^c Only the configuration interaction coefficients that are equal or larger than 0.30 of the corresponding natural orbital representations are reported. ^d β and α -spin electrons are specified with and without bars over the spatial orbital, respectively.

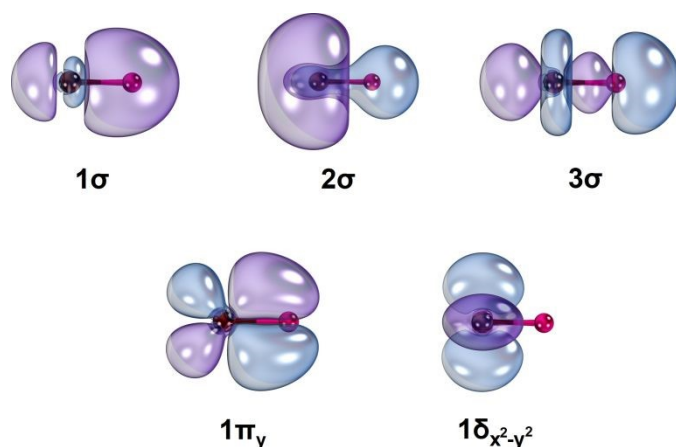


Figure 2. Select QZ-CASSCF state-average orbitals of ThBe at $r_e = 2.65$ Å. The Th and Be atoms of each orbital plot are shown in wine and red, respectively. All studied 13 electronic states of ThBe were used to produce the orbitals. The two phases of orbitals are given in purple and blue. The rotations of $1\pi_y$ and $1\delta_{x^2-y^2}$ orbitals by 90° and 45° along the z-axis (Th–Be bond) produce the contours of $1\pi_x$ and $1\delta_{xy}$, respectively. The IboView⁶⁴ software was used to produce molecular orbitals.

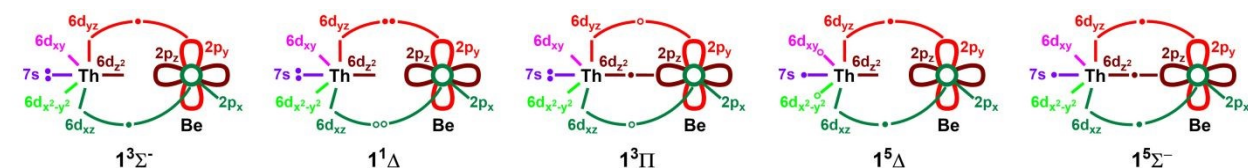


Figure 3. Proposed vbL diagrams for the first 5 electronic states of ThBe. In each case, the 2s orbital of Be is doubly occupied and not depicted for clarity. The $1\pi_x^2 \pm 1\pi_y^2$ combinations of $1^1\Delta$ are represented with electron pairs shown by solid ($1\pi_y^2$) and open circles ($1\pi_x^2$). Open circles are used to illustrate the different components of each $1^3\Pi$ and $1^5\Delta$ where either one of the two open circles is populated by an electron. Table 1 lists their exact electronic configurations.

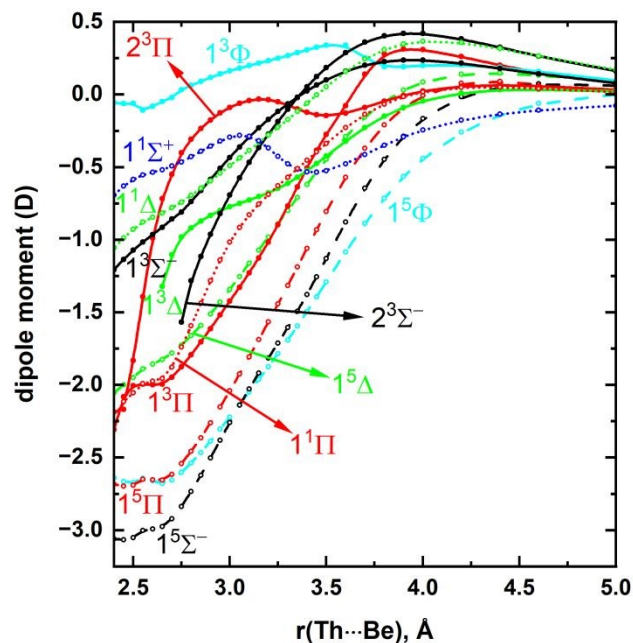


Figure 4. QZ-MRCI DMC of ThBe as a function of Th...Be distance [$r(\text{Th}\cdots\text{Be})$, Å]. The Σ^+ , Σ^- , Π , Δ , and Φ states are shown in blue, black, red, green, and cyan, respectively. The dashed, solid, and dotted PECs correspond to the quintet, triplet, and singlet spin electronic states, respectively.



The calculated spectroscopic parameters of the 13 electronic states of ThBe are listed in Table 2. Note that the single-reference coupled-cluster calculations were only performed for the $1^3\Sigma^-$ and $1^3\Pi$ electronic states of ThBe which are the two most stable single-reference electronic states of ThBe. The QZ-MRCI predicted T_e of $1^1\Delta$ is $\sim 260\text{ cm}^{-1}$ lower compared to its QZ-MRCI+Q T_e (Table 2). At the QZ-MRCI and QZ-MRCI+Q levels, the next excited state of ThBe (i.e., $1^3\Pi$) lies 17 and 395 cm^{-1} above the $1^1\Delta$. The QZ-MRCI+Q T_e of $1^3\Pi$ is relatively closer to its coupled-cluster T_e value than the QZ-MRCI T_e (discrepancies between QZ-MRCI+Q versus coupled cluster is $347\text{--}465\text{ cm}^{-1}$: Table 2). The utilization of all electron basis set decreased the T_e of $1^3\Pi$ only by 32 cm^{-1} (compare QZ-CCSD(T) and QZ-A-CCSD(T) values of Table 2). Based on the coupled-cluster findings, the $5d^{10}$ core electron correlation of Th atom increased the T_e of $1^3\Pi$ by 88 cm^{-1} . Under the composite level of theoretical approach utilized in this work [i.e., CBS-C-CCSD(T)+ $\delta T(Q)$], the T_e of $1^3\Pi$ is 2887 cm^{-1} which is 347 cm^{-1} lower than the QZ-MRCI+Q value. Overall, at the QZ-MRCI+Q level, the order of the electronic states of ThBe is $1^3\Sigma^-$, $1^1\Delta$, $1^3\Pi$, $1^5\Delta$, $1^5\Sigma^-$, $1^3\Phi$, $1^1\Sigma^+$, $2^3\Pi$, $1^1\Pi$, $1^5\Phi$, $1^5\Pi$, $1^3\Delta$, and $2^3\Sigma^-$. The QZ-MRCI order of the states is similar to the QZ-MRCI+Q except for the $2^3\Pi$ being more stable than the $1^1\Sigma^+$ at the QZ-MRCI level. For all states, the QZ-MRCI+Q predicted shorter r_e values compared to the QZ-MRCI (Table 2). The core electron correlation slightly decreased the r_e values of both $1^3\Sigma^-$ and $1^3\Pi$ states, which is commonly observed in the literature.^{65–69} The QZ-A-CCSD(T) r_e values are slightly longer compared to the QZ-CCSD(T) (by 0.006 and 0.005 \AA for $1^3\Sigma^-$ and $1^3\Pi$, respectively). The QZ-A-CCSD(T) predicted slightly lower ω_e and $\omega_e x_e$ compared to the QZ-CCSD(T) values (Table 2).

Table 2. Adiabatic excitation energy T_e (cm^{-1}), bond length r_e (\AA), harmonic vibrational frequency ω_e (cm^{-1}), and anharmonicity $\omega_e x_e$ (cm^{-1}) of 13 low-lying electronic states of ThBe and the bond dissociation energy of $1^3\Sigma^-$ with respect to the $\text{Th}(^3\text{F}; 6d^2 7s^2) + \text{Be}(^1\text{S}; 2s^2)$ fragments (D_0 , kcal/mol).

State	Level of theory ^a	T_e	r_e	ω_e	$\omega_e x_e$	D_0
$1^3\Sigma^-$	CBS-C-CCSD(T)+ $\delta T(Q)$	0	-	-	-	20.72
	CBS-C-CCSD(T)	0	2.629	375	3.7	18.71
	QZ-C-CCSD(T)	0	2.634	375	3.7	18.47
	TZ-C-CCSD(T)	0	2.643	375	3.8	18.06
	QZ-A-CCSD(T)	0	2.643	370	3.7	17.59
	QZ-CCSD(T)	0	2.637	375	3.9	18.19
	QZ-MRCI+Q	0	2.639	376	4.0	20.25
	QZ-MRCI	0	2.661	364	4.1	17.67
$1^1\Delta$	QZ-MRCI+Q	2145	2.678	383	4.9	
	QZ-MRCI	2403	2.702	368	4.9	
$1^3\Pi$	CBS-C-CCSD(T)+ $\delta T(Q)$	2887	-	-	-	
	CBS-C-CCSD(T)	2999	2.770	347	4.8	
	QZ-C-CCSD(T)	3000	2.775	345	5.1	
	TZ-C-CCSD(T)	3005	2.786	341	5.4	
	QZ-A-CCSD(T)	2880	2.790	338	5.2	
	QZ-CCSD(T)	2912	2.785	341	5.3	
	QZ-MRCI+Q	2540	2.793	324	6.5	



	QZ-MRCI	2420	2.799	330	6.6
$1^5\Delta$	QZ-MRCI+Q	2785	2.629	379	6.5
	QZ-MRCI	2955	2.654	382	7.1
$1^5\Sigma^-$	QZ-MRCI+Q	3476	2.587	455	8.2
	QZ-MRCI	3496	2.588	462	8.4
$1^3\Phi$	QZ-MRCI+Q	3951	2.933	630	4.5
	QZ-MRCI	3736	2.974	257	4.9
$1^1\Sigma^+$	QZ-MRCI+Q	3967	2.699	350	2.4
	QZ-MRCI	4226	2.717	360	2.8
$2^3\Pi$	QZ-MRCI+Q	4010	2.887	269	6.1
	QZ-MRCI	3857	2.920	284	6.6
$1^1\Pi$	QZ-MRCI+Q	4439	2.825	317	5.1
	QZ-MRCI	4354	2.834	294	4.8
$1^5\Phi$	QZ-MRCI+Q	4646	2.776	380	2.4
	QZ-MRCI	4628	2.790	369	2.1
$1^5\Pi$	QZ-MRCI+Q	5381	2.773	354	6.5
	QZ-MRCI	5348	2.785	335	7.3
$1^3\Delta$	QZ-MRCI+Q	5426	3.139	198	3.8
	QZ-MRCI	5329	3.212	187	3.3
$2^3\Sigma^-$	QZ-MRCI+Q	6590	3.166	184	8.2
	QZ-MRCI	6320	3.262	168	7.5

^a Davidson corrected MRCI is denoted by MRCI+Q. TZ = cc-pVTZ of Be and cc-pVTZ-PP of Th. QZ = cc-pVQZ of Be and cc-pVQZ-PP of Th. QZ-A = cc-pVQZ-DK of Be and cc-pVQZ-DK3 of Th. TZ-C = cc-pVTZ of Be and cc-pwCVTZ-PP of Th. QZ-C = cc-pVQZ of Be and cc-pwCVQZ-PP of Th. See Computational details section for more information on basis sets.

The QZ-MRCI+Q D_0 of ThBe ($1^3\Sigma^-$) is 20.25 kcal/mol which is 2.58 kcal/mol larger than the QZ-MRCI value. The QZ-MRCI+Q D_0 value is only 0.47 kcal/mol lower compared to its D_0 predicted by CBS-C-CCSD(T)+ δ T(Q) which is the largest coupled-cluster approach that does not account for spin-orbit coupling (Table 2). Since the spin-orbit effects must be accounted for in order to reach accurate predictions on actinide diatomic species, next, this effects of ThBe were calculated at the QZ-MRCI+Q level at the 2.629 Å which is the CBS-C-CCSD(T) r_e of the $1^3\Sigma^-$ of ThBe. To construct the spin-orbit matrix of this calculation all the 13 electronic states listed in Table 2 were used. The Ω states resulting from these 13 electronic states ThBe are given in the ESI Table S1. The vertical excitation energies and the AS compositions of 23 spin-orbit states of ThBe are reported in Table 3. The ground spin-orbit state of ThBe is an $\Omega = 0^+$ which is dominantly $1^3\Sigma^-$ (86%) with minor $1^3\Pi$ (9%), $1^1\Sigma^+$ (3%), and $2^3\Pi$ (2%). The $\Omega = 1$ of $1^3\Sigma^-$ lies 266 cm^{-1} above the ground $\Omega = 0^+$. Overall, the spin-orbit effect accounted spectrum of ThBe is highly dense and complicated due to the many AS mixings. Overall, the spin-orbit effects considerably decreased the D_0 of ThBe. Specifically, at the QZ-MRCI+Q-SO the D_0 of ThBe ($1^3\Sigma^-_{0^+}$) is 12.92 kcal/mol which is 7.33 kcal/mol lower than its D_0 at QZ-MRCI+Q D_0 . The inclusion of this spin-orbit correction to the CBS-C-CCSD(T)+ δ T(Q) D_0 of ThBe ($1^3\Sigma^-$) resulted in 13.39 kcal/mol D_0 [CBS-C-CCSD(T)+ δ T(Q)+ δ SO]. Considering D_0 values of ThBe ($1^3\Sigma^-$) under QZ-CCSD(T) and QZ-A-CCSD(T) levels we can estimate an ECP error of 0.6 kcal/mol. Inclusion of this D_0 to our CBS-C-CCSD(T)+ δ T(Q)+ δ SO D_0 provided a 12.79 kcal/mol D_0 for ThBe ($1^3\Sigma^-_{0^+}$).



Finally, the D_0 of ThBe ($1^3\Sigma^-_{0+}$) [i.e., 12.79 kcal/mol or 53.51 kJ/mol], $\Delta H_f^\circ(0\text{ K, Th})$ (i.e., 602 ± 6 kJ/mol)⁷⁰ and $\Delta H_f^\circ(0\text{ K, Be})$ (i.e., 320.03 kJ/mol)⁷¹ were used to calculate $\Delta H_f^\circ(0\text{ K, ThBe})$ via, $\Delta H_f^\circ(0\text{ K, ThBe}) = \Delta H_f^\circ(0\text{ K, Th}) + \Delta H_f^\circ(0\text{ K, Be}) - D_0(\text{ThBe})$. The calculated $\Delta H_f^\circ(0\text{ K, ThBe})$ is 868.52 ± 6 kJ/mol. The QZ-A-CCSD(T) level predicted a $H^\circ(298\text{ K, ThBe}) - H^\circ(0\text{ K, ThBe})$ of 9.55 kJ/mol. Using this value and the thermal corrections of 6.51 and 1.95 kJ/mol for Th [i.e., $H^\circ(298\text{ K, Th}) - H^\circ(0\text{ K, Th})$]⁷¹ and Be [i.e., $H^\circ(298\text{ K, Be}) - H^\circ(0\text{ K, Be})$]⁷¹, the $\Delta H_f^\circ(298\text{ K, ThBe})$ of 869.61 ± 6 kJ/mol was calculated using, $\Delta H_f^\circ(298\text{ K, ThBe}) = \Delta H_f^\circ(0\text{ K, ThBe}) + [H^\circ(298\text{ K, ThBe}) - H^\circ(0\text{ K, ThBe})] - [H^\circ(298\text{ K, Th}) - H^\circ(0\text{ K, Th})] - [H^\circ(298\text{ K, Be}) - H^\circ(0\text{ K, Be})]$.⁷²

Table 3. Vertical excitation energy ΔE (cm^{-1}) and % AS composition of 23 spin-orbit states of ThBe at the QZ-MRCI+Q level of theory. ^a

Ω	ΔE	% AS composition
0 ⁺	0	86% $1^3\Sigma^-$ + 9% $1^3\Pi$ + 3% $1^1\Sigma^+$ + 2% $2^3\Pi$
1	266	94% $1^3\Sigma^-$ + 3% $1^3\Pi$ + 1% $2^3\Pi$ + 1% $1^1\Pi$
2	1581	58% $1^1\Delta$ + 23% $1^3\Pi$ + 10% $1^3\Phi$ + 7% $1^5\Sigma^-$ + 1% $1^5\Delta$
0 ⁻	1976	92% $1^5\Delta$ + 3% $1^5\Pi$ + 2% $1^5\Sigma^-$ + 2% $1^3\Pi$
0 ⁺	2000	97% $1^5\Delta$ + 2% $1^5\Pi$
1	2363	75% $1^5\Delta$ + 7% $1^3\Pi$ + 6% $1^5\Phi$ + 6% $1^5\Sigma^-$ + 4% $1^5\Pi$ + 1% $2^3\Pi$
0 ⁻	2629	65% $1^3\Pi$ + 27% $1^5\Sigma^-$ + 6% $1^5\Delta$ + 2% $1^5\Pi$
1	2750	45% $1^3\Pi$ + 32% $1^5\Sigma^-$ + 14% $1^5\Delta$ + 2% $1^5\Phi$ + 2% $1^5\Pi$ + 2% $1^1\Pi$ + 1% $1^3\Sigma^-$ + 1% $1^3\Pi$
2	2944	86% $1^5\Delta$ + 8% $1^5\Phi$ + 3% $1^5\Pi$ + 2% $1^1\Delta$
2	3025	40% $1^5\Sigma^-$ + 21% $1^3\Pi$ + 14% $1^3\Phi$ + 11% $1^1\Delta$ + 10% $1^5\Delta$ + 3% $1^5\Phi$
0 ⁺	3121	74% $1^3\Pi$ + 11% $1^1\Sigma^+$ + 10% $1^3\Sigma^-$ + 3% $2^3\Pi$ + 1% $1^5\Delta$
3	3541	88% $1^5\Delta$ + 8% $1^5\Phi$ + 2% $1^3\Phi$ + 2% $1^5\Pi$
0 ⁻	4001	46% $1^5\Sigma^-$ + 29% $1^3\Pi$ + 14% $2^3\Pi$ + 9% $1^5\Pi$ + 1% $1^5\Delta$
1	4121	90% $1^5\Phi$ + 7% $1^5\Delta$ + 1% $1^5\Pi$ + 1% $1^3\Pi$
4	4251	93% $1^5\Delta$ + 5% $1^5\Phi$ + 2% $1^3\Phi$
1	4323	40% $1^5\Sigma^-$ + 37% $1^3\Pi$ + 11% $1^5\Pi$ + 4% $2^3\Pi$ + 4% $1^1\Pi$ + 1% $1^5\Delta$
0 ⁺	4444	51% $2^3\Pi$ + 36% $1^1\Sigma^+$ + 12% $1^3\Pi$ + 1% $1^3\Sigma^-$
2	4613	50% $1^3\Phi$ + 16% $1^5\Phi$ + 14% $1^5\Sigma^-$ + 9% $1^1\Delta$ + 7% $1^5\Delta$ + 4% $1^3\Pi$
0 ⁻	4847	85% $2^3\Pi$ + 10% $1^5\Sigma^-$ + 4% $1^3\Pi$ + 1% $1^5\Pi$
1	4928	72% $2^3\Pi$ + 12% $1^1\Pi$ + 4% $1^3\Delta$ + 4% $2^3\Sigma^-$ + 3% $1^5\Sigma^-$ + 3% $1^3\Sigma^-$ + 1% $1^5\Pi$
2	4985	47% $1^5\Phi$ + 20% $1^3\Pi$ + 15% $2^3\Pi$ + 9% $1^5\Sigma^-$ + 4% $1^3\Phi$ + 2% $1^5\Delta$ + 1% $1^5\Pi$ + 1% $1^3\Delta$
2	5170	34% $2^3\Pi$ + 29% $1^5\Phi$ + 16% $1^3\Phi$ + 9% $1^3\Pi$ + 6% $1^1\Delta$ + 2% $1^5\Delta$ + 2% $1^3\Delta$ + 1% $1^5\Sigma^-$
0 ⁺	5243	47% $1^1\Sigma^+$ + 39% $2^3\Pi$ + 5% $1^5\Pi$ + 3% $1^3\Pi$ + 3% $1^3\Sigma^-$ + 2% $2^3\Sigma^-$

^a ΔE values and corresponding % AS compositions were computed at the $r_e = 2.629\text{ \AA}$, which is the CBS-C-CCSD(T) r_e of the ThBe($1^3\Sigma^-$). The cc-pVQZ of Be and cc-pVQZ-PP of Th basis set (QZ) was used for the MRCI+Q spin-orbit calculation.

IIIB. AcBe

To investigate the low-lying electronic states of AcBe, the Ac(2D ; $6d^17s^2$)+Be($1S$; $2s^2$), Ac($^2P^\circ$; $7s^27p^1$)+Be($1S$; $2s^2$), Ac(4F ; $6d^27s^1$)+Be($1S$; $2s^2$), Ac($^4F^\circ$; $6d^17s^17p^1$)+Be($1S$; $2s^2$), Ac(4P ; $6d^27s^1$)+Be($1S$; $2s^2$), and Ac($^2D^\circ$; $6d^17s^17p^1$)+Be($1S$; $2s^2$) asymptotes were considered.³¹ Specifically, at the CASSCF level all PECs of the aforementioned atomic combinations were investigated. Then the most stable



electronic states of AcBe were studied at the QZ-MRCI+Q level of theory (Figure 5). The $\text{Ac}(^2\text{D})+\text{Be}(^1\text{S})$ ground state fragments produce $^2[\Sigma^+, \Pi, \Delta]$ molecular states of AcBe. This reaction gives rise to the ground state ($1^2\Pi$) and the first excited state ($1^2\Sigma^+$) of AcBe (Figure 5). The $1^2\Delta$ PEC of the ground state fragments is only slightly attractive (by ~ 2 kcal/mol) with a minimum around 3.7 Å. This $1^2\Delta$ PEC displays a shoulder around 2.9 Å due to its interaction with the $2^2\Delta$ of AcBe. The second excited state of AcBe (i.e., $1^4\Sigma^+$) originating from the $\text{Ac}(^4\text{F})+\text{Be}(^1\text{S})$ asymptote is ~ 4 kcal/mol stable with respect to the ground state fragments. The $^4\Pi$ and $^4\Phi$ molecular states of the same reactants create the 5th and 6th excited electronic states of the system. Note that the PECs arising from $\text{Ac}(^2\text{P}^0; 7s^2 7p^1)+\text{Be}(^1\text{S}; 2s^2)$ atomic combination that fall in between $\text{Ac}(^2\text{D}; 6d^1 7s^2)+\text{Be}(^1\text{S}; 2s^2)$ and $\text{Ac}(^4\text{F}; 6d^2 7s^1)+\text{Be}(^1\text{S}; 2s^2)$ asymptotes do not produce stable minima and hence are not given in Figure 5. Both 4th and 7th excited states of AcBe are results of the highest energy fragments that were considered here [i.e., $\text{Ac}(^2\text{D}^0; 6d^1 7s^1 7p^1)+\text{Be}(^1\text{S}; 2s^2)$].

The ground state of AcBe ($1^2\Pi$) has a $1\sigma^2 2\sigma^2 1\pi^1$ electron configuration which accounts for a bond-order of 0.5 (Table 4 and Figure 6). This lower bond-order rationalizes its relatively less strong chemical bond (i.e., the $1^2\Pi$ is only bound by ~ 10 kcal/mol with respect to ground state fragments). Addition of an electron to the vacant 1π orbital of AcBe ($1^2\Pi$) gives rise to the ground electron configuration of the ThBe ($1^3\Sigma^-; 1\sigma^2 2\sigma^2 1\pi^2$). According to the NBO analysis, the AcBe ($1^2\Pi$) carries $\text{Ac}[6d^{0.74} 7s^{1.95} 5f^{0.12} 7p^{0.17}]\text{Be}[2s^{1.83} 2p^{0.17}]$ electron population. This electron population closely resembles the electron configurations of its reactants [i.e., $\text{Ac}(^2\text{D}; 6d^1 7s^2)+\text{Be}(^1\text{S}; 2s^2)$] which again correlates to the less strong chemical bond of AcBe ($1^2\Pi$). The electron transfer from 1π of AcBe ($1^2\Pi$) to the empty 3σ creates its first excited state [i.e., $1^2\Sigma^+$] (Table 4 and Figure 6). The absence of the shared electrons between Ac and Be addresses the shallow minimum of the AcBe [$1^2\Delta; 1\sigma^2 2\sigma^2 1\delta^1$]. Both $1^4\Sigma^+$ and $1^2\Sigma^+$ host two electrons in 1π orbitals hence each of their bond orders add up to 1 which translates to their short r_e values.



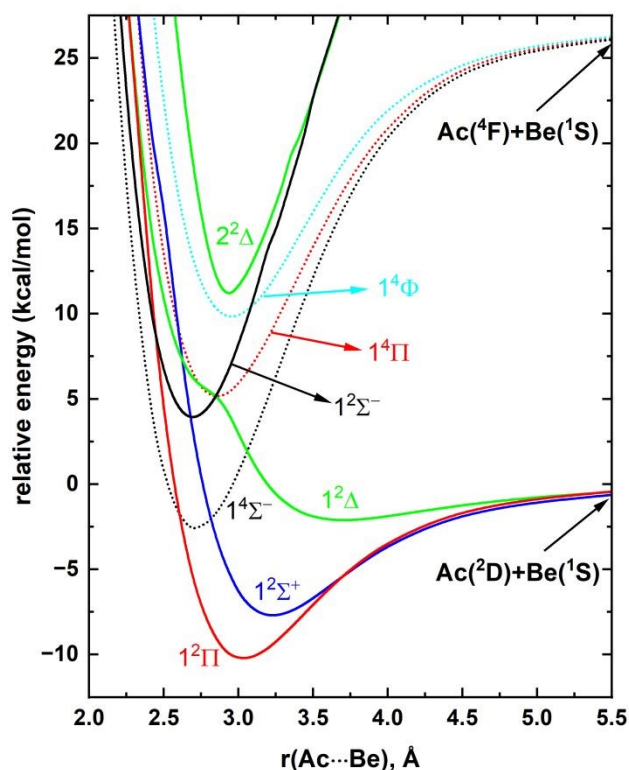


Figure 5. QZ-MRCI+Q PECs of AcBe as a function of Ac...Be distance [$r(\text{Ac}\cdots\text{Be})$, Å]. The relative energies are referenced to the dissociation limit of $\text{Ac}(^2\text{D}) + \text{Be}(^1\text{S})$, which is set to 0 kcal/mol. The Σ^+ , Σ^- , Π , Δ , and Φ states are shown in blue, black, red, green, and cyan, respectively. The dotted and solid PECs correspond to the quartet and doublet spin electronic states, respectively.

Table 4. Dominant electronic configurations at equilibrium distances of the studied electronic states of AcBe.^a

State ^b	Coefficient ^c	Configuration ^d
$1^2\Pi$	0.88	$1\sigma^2 2\sigma^2 1\pi_x$
$1^2\Sigma^+$	0.86	$1\sigma^2 2\sigma^2 3\sigma$
$1^4\Sigma^-$	0.90	$1\sigma^2 2\sigma 1\pi_x 1\pi_y$
$1^2\Delta$	0.86	$1\sigma^2 2\sigma^2 (1\delta_{x^2-y^2})$
$1^2\Sigma^-$	0.73	$1\sigma^2 2\sigma 1\pi_x 1\pi_y$
	-0.36	$1\sigma^2 2\sigma 1\pi_x 1\pi_y$
	-0.36	$1\sigma^2 2\sigma 1\pi_x 1\pi_y$
$1^4\Pi$	0.83	$1\sigma^2 2\sigma 3\sigma 1\pi_x$
$1^4\Phi$	0.66	$1\sigma^2 2\sigma 1\pi_x (1\delta_{x^2-y^2})$
	0.66	$1\sigma^2 2\sigma 1\pi_y 1\delta_{xy}$
$2^2\Delta$	-0.54	$1\sigma^2 2\sigma 1\pi_y^2$
	0.54	$1\sigma^2 2\sigma 1\pi_x^2$
	-0.32	$1\sigma^2 2\sigma^2 (1\delta_{x^2-y^2})$

^a The coefficients and electron configurations were collected under state-average QZ-CASSCF that includes all listed 8 electronic states of AcBe. ^b The B_1 components of Π and Φ states and A_1 of the Δ states under C_{2v} symmetry are listed. ^c Only the configuration interaction coefficients that are equal or larger than 0.30 of the corresponding natural orbital representations are reported. ^d β and α -spin electrons are specified with and without bars over the spatial orbital, respectively.



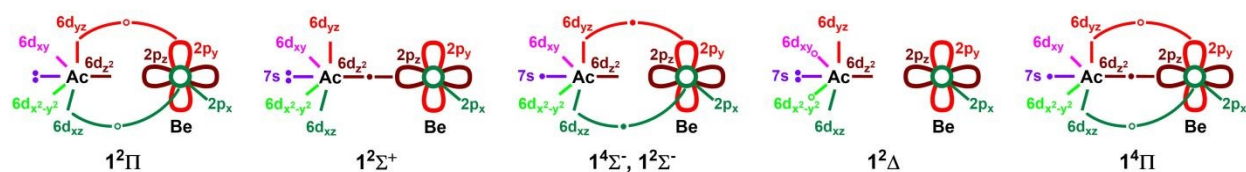


Figure 6. Proposed vbL diagrams for the first 6 electronic states of AcBe. In each case, the 2s orbital of Be is doubly occupied and not shown for clarity. Open circles are used to illustrate the different components of each $1^2\Pi$, $1^2\Delta$, and $1^4\Pi$ where either one of the two open circles is populated by an electron. Table 4 lists their exact electronic configurations.

The spectroscopic parameters of the studied 8 electronic states of AcBe are given in Table 5. At QZ-MRCI+Q, the order of the electronic states of AcBe is $1^2\Pi$, $1^2\Sigma^+$, $1^4\Sigma^-$, $1^2\Delta$, $1^2\Sigma^-$, $1^4\Pi$, $1^4\Phi$, and $2^2\Delta$. The QZ-MRCI order of the states are the same as the QZ-MRCI+Q order except for the swapping of the $1^4\Sigma^-$ and $1^2\Delta$. Specifically, QZ-MRCI predicted the $1^2\Delta$ to be more stable than the $1^4\Sigma^-$ by 461 cm^{-1} . Similar to the ThBe case, QZ-MRCI+Q predicted shorter r_e values compared to the QZ-MRCI r_e values (Table 5). For r_e values, the largest discrepancy between QZ-MRCI+Q versus QZ-MRCI was observed for the weakly bonded $1^2\Delta$ (i.e., 3.697 versus 3.916 \AA). The coupled-cluster spectroscopic parameters were only calculated for the AcBe ($1^2\Pi$) and these r_e values agree well with the QZ-MRCI+Q value (Table 5). Similarly, the QZ-MRCI+Q D_0 of AcBe ($1^2\Pi$) is closer to the coupled-cluster values than the QZ-MRCI values. Specifically, the D_0 of AcBe ($1^2\Pi$) at QZ-MRCI, QZ-MRCI+Q, and coupled-cluster levels are 8.16, 9.55, and 10.66–11.42 kcal/mol, respectively (Table 5). Indeed, the largest D_0 of AcBe (i.e., 11.42 kcal/mol) was predicted by the highest level of spin-orbit effect free theoretical approach CBS-C-CCSD(T)+ $\delta T(Q)$. It should be noted that the spin-orbit effects of AcBe were evaluated utilizing the Breit-Pauli Hamiltonian which is compatible with the all electron basis sets. The Ω states originating from the electronic states AcBe are given in the ESI Table S2. The spin-orbit effects were found to be minor for the D_0 of AcBe. Specifically, at the QZ-MRCI+Q level of theory, the spin-orbit coupling effects only decreased the D_0 of AcBe by 0.4 kcal/mol. Utilizing this energy correction, we predicted our final D_0 of 11.02 kcal/mol [at the CBS-C-CCSD(T)+ $\delta T(Q)$ + δSO approach] for its spin-orbit ground state ($\Omega = 1/2$). The spin-orbit ground state of AcBe ($\Omega = 1/2$) is primarily $1^2\Pi$ (87%) with a 12% of $1^2\Sigma^+$. The $\Omega = 3/2$ of $1^2\Pi$ is the first excited spin-orbit state of AcBe lying 1097 cm^{-1} above the $1^2\Pi_{1/2}$ ground state. Next, we observed the $1^2\Sigma^+_{1/2}$, $1^4\Sigma^-_{1/2}$, $1^2\Delta_{3/2}$, $1^4\Sigma^-_{3/2}$, $1^2\Delta_{5/2}$, and $1^4\Pi_{1/2}$ spin-orbit states of AcBe spanned within $2050\text{--}6050\text{ cm}^{-1}$. Overall, the spin-orbit spectrum of AcBe is much resolved and less complex compared to the spin-orbit spectrum of ThBe (Tables 3 and 6).



Table 5. Adiabatic excitation energy T_e (cm^{-1}), bond length r_e (\AA), harmonic vibrational frequency ω_e (cm^{-1}), and anharmonicity $\omega_e x_e$ (cm^{-1}) of 8 low-lying electronic states of AcBe and the bond dissociation energy of $1^2\Pi$ with respect to the $\text{Ac}(^2\text{D}; 6\text{d}^1 7\text{s}^2) + \text{Be}(^1\text{S}; 2\text{s}^2)$ fragments (D_0 , kcal/mol).

State	Level of theory ^a	T_e	r_e	ω_e	$\omega_e x_e$	D_0
$1^2\Pi$	CBS-C-CCSD(T)+ $\delta\text{T}(\text{Q})$	0	-	-	-	11.42
	CBS-C-CCSD(T)	0	3.025	272	4.7	11.36
	QZ-C-CCSD(T)	0	3.029	270	4.7	11.08
	TZ-C-CCSD(T)	0	3.036	268	4.8	10.66
	QZ-CCSD(T)	0	3.037	264	4.8	10.69
	QZ-MRCI+Q	0	3.036	273	4.2	9.55
	QZ-MRCI	0	3.055	270	4.3	8.16
$1^2\Sigma^+$	QZ-MRCI+Q	879	3.227	237	3.3	
	QZ-MRCI	1016	3.238	225	3.5	
$1^4\Sigma^-$	QZ-MRCI+Q	2645	2.702	398	2.5	
	QZ-MRCI	3118	2.707	397	2.7	
$1^2\Delta$	QZ-MRCI+Q	2835	3.697	98	3.1	
	QZ-MRCI	2657	3.916	67	5.0	
$1^2\Sigma^-$	QZ-MRCI+Q	4936	2.694	409	2.3	
	QZ-MRCI	5556	2.702	404	2.1	
$1^4\Pi$	QZ-MRCI+Q	5367	2.854	345	2.6	
	QZ-MRCI	5714	2.857	355	3.0	
$1^4\Phi$	QZ-MRCI+Q	7006	2.952	308	2.1	
	QZ-MRCI	7367	2.960	312	2.3	
$2^2\Delta$	QZ-MRCI+Q	7460	2.937	506	6.6	
	QZ-MRCI	8075	2.942	503	7.1	

^a Davidson corrected MRCI is denoted by MRCI+Q. TZ = cc-pVTZ-DK of Be and cc-pVTZ-DK3 of Ac. QZ = cc-pVQZ-DK of Be and cc-pVQZ-DK3 of Ac. TZ-C = cc-pVTZ-DK of Be and cc-pwCVTZ-DK3 of Ac. QZ-C = cc-pVQZ-DK of Be and cc-pwCVQZ-DK3 of Ac. See Computational details section for more information on basis sets.

Table 6. Vertical excitation energy ΔE (cm^{-1}) and % ΛS composition of 8 spin-orbit states of AcBe at the QZ-MRCI+Q level of theory. ^a

Ω	ΔE	% ΛS composition
1/2	0	87% $1^2\Pi$ + 12% $1^2\Sigma^+$
3/2	1097	97% $1^2\Pi$ + 1% $1^4\Sigma^-$ + 1% $1^2\Delta$
1/2	2057	86% $1^2\Sigma^+$ + 13% $1^2\Pi$ + 1% $1^4\Pi$
1/2	4460	86% $1^4\Sigma^-$ + 13% $1^4\Pi$ + 1% $1^2\Sigma^+$
3/2	4638	72% $1^2\Delta$ + 27% $1^4\Sigma^-$
3/2	4670	65% $1^4\Sigma^-$ + 26% $1^2\Delta$ + 6% $1^4\Pi$ + 3% $1^2\Pi$
5/2	5614	91% $1^2\Delta$ + 6% $1^4\Pi$ + 2% $2^2\Delta$
1/2	6041	91% $1^4\Pi$ + 7% $1^2\Sigma^-$ + 1% $1^4\Sigma^-$

^a ΔE values and corresponding % ΛS compositions were computed at the $r_e = 3.025 \text{ \AA}$, which is the CBS-C-CCSD(T) r_e of the $\text{AcBe}(1^2\Pi)$. The cc-pVQZ-DK of Be and cc-pVQZ-DK3 of Ac (QZ) was used for the MRCI+Q spin-orbit calculation.

IV. CONCLUSIONS



In conclusion, the MRCI, MRCI+Q, CCSD(T), and CCSDT(Q) *ab initio* quantum chemical calculations were performed under correlation consistent basis sets to study the spin-free and spin-orbit states of ThBe and AcBe species. First, at the QZ-MRCI+Q level, the full PECs of 13 and 8 electronic states of ThBe and AcBe, respectively, were calculated. These QZ-MRCI+Q PECs and corresponding QZ-MRCI PECs were used to calculate their T_e , r_e , ω_e , and $\omega_e x_e$ spectroscopic parameters. Based on the equilibrium electron configurations and the shapes of the occupied molecular orbitals, chemical bonding patterns of low-lying electronic states of ThBe and AcBe were proposed. The ground electronic states of ThBe and AcBe are $1^3\Sigma^-$ and $1^2\Pi$, and bear $1\sigma^2 2\sigma^2 1\pi^2$ and $1\sigma^2 2\sigma^2 1\pi^1$ equilibrium electronic configurations, respectively. The equilibrium electron populations of Th[6d^{1.98}7s^{1.91}5f^{0.19}7p^{0.17}]Be[2s^{1.65}2p^{0.09}] of ThBe ($1^3\Sigma^-$) and Ac[6d^{0.74}7s^{1.95}5f^{0.12}7p^{0.17}]Be[2s^{1.83}2p^{0.17}] of AcBe ($1^2\Pi$) demonstrate their leading “transition-metal-like” characters. Both ThBe($1^3\Sigma^-$) and AcBe($1^2\Pi$) smoothly dissociate to their Th(3F ; 6d²7s²)+Be($1S$; 2s²) and Ac(2D ; 6d¹7s²)+Be($1S$; 2s²) ground state fragments. With respect to the ground state fragments, the ThBe($1^3\Sigma^-$) and AcBe($1^2\Pi$) bear 18.71 and 11.36 kcal/mol D_0 values at the CBS-C-CCSD(T) level, respectively. The $\delta T(Q)$ higher-order electron correlation was found to be significant for ThBe($1^3\Sigma^-$) which increased the D_0 by 2.01 kcal/mol, whereas the $\delta T(Q)$ effect for the D_0 of AcBe($1^2\Pi$) is as minor as 0.06 kcal/mol. The spin-orbit ground states of ThBe and AcBe are $\Omega = 0^+$ and $\Omega = 1/2$ with dominant $1^3\Sigma^-$ (86%) + $1^3\Pi$ (9%) and $1^2\Pi$ (87%) + $1^2\Sigma^+$ (12%) characters, respectively. The spin-orbit effect accounted final estimates of D_0 of ThBe ($1^3\Sigma^-_{0+}$) and AcBe ($1^2\Pi_{1/2}$) are 12.79 and 11.02 kcal/mol, respectively. The D_0 of ThBe was used to estimate its ΔH_f° (298 K) of 869.61 ± 6 kJ/mol. The spectrum of AcBe is significantly less dense compared to the spectrum of ThBe. Specifically, AcBe and ThBe populated 8 and 23 spin-orbit states within 0-6041 and 0-5243 cm⁻¹, respectively. Overall, we believe the theoretical findings reported here will be of great use for future experimental spectroscopic studies of ThBe and AcBe.

V. ACKNOWLEDGEMENTS

The support of the Los Alamos National Laboratory (LANL) Laboratory Directed Research and Development program Project No. 20240737PRD1 is acknowledged. This research used resources provided by the Los Alamos National Laboratory Institutional Computing Program, which is supported by the U.S. Department of Energy National Nuclear Security Administration under Contract No. 89233218CNA000001.



VI. CONFLICTS OF INTEREST

There are no conflicts to declare.

VII. ELECTRONIC SUPPLEMENTARY INFORMATION (ESI) AVAILABLE

Figure S1 illustrates the transition dipole moment curves of ThBe; Table S1 lists the Ω states of electronic states of ThBe; Table S2 lists the Ω states of electronic states of AcBe

VIII. REFERENCES

1. M. Pepper and B. E. Bursten, *Chemical Reviews*, 1991, **91**, 719-741.
2. P. Pyykko, *Annu Rev Phys Chem*, 2012, **63**, 45-64.
3. M. C. Heaven and K. A. Peterson, *Probing Actinide Bonds in the Gas Phase, Chapter 1 in Experimental and Theoretical Approaches to Actinide Chemistry*, John Wiley & Sons Ltd, 2018.
4. I. R. Ariyaratna, J. A. Leiding, A. J. Neukirch and M. C. Zammit, *J Phys Chem A*, 2024, **128**, 9412-9425.
5. I. R. Ariyaratna and E. Miliordos, *Physical Chemistry Chemical Physics*, 2018, **20**, 12278-12287.
6. I. R. Ariyaratna, C. Duan and H. J. Kulik, *The Journal of Chemical Physics*, 2022, **156**, 184113.
7. N. M. S. Almeida, T. R. L. Melin and A. K. Wilson, *J Chem Phys*, 2021, **154**, 244304.
8. S. C. North, N. M. S. Almeida, T. R. L. Melin and A. K. Wilson, *J Phys Chem A*, 2023, **127**, 107-121.
9. *Actinide Research Quarterly* Los Alamos National Laboratory, 2004, https://cdn.lanl.gov/files/arq-2004-spring_045b6.pdf.
10. H.-S. Hu, X.-C. Xu, C.-Q. Xu and J. Li, *Chinese J. Struct. Chem*, 2020, **39**, 1201-1212.
11. A. Pichon, *Nature Chemistry*, 2017, **9**, 832-832.
12. M. L. Neidig, D. L. Clark and R. L. Martin, *Coordination Chemistry Reviews*, 2013, **257**, 394-406.
13. J. G. F. Romeu, G. F. de Melo, K. A. Peterson and D. A. Dixon, *J Phys Chem A*, 2025, **129**, 3763-3779.
14. P. D. Wilson, *The Nuclear Fuel Cycle: From Ore to Waste*, Oxford University Press, 1996.
15. Stages of the Nuclear Fuel Cycle, U.S. Nuclear Regulatory Commission, <https://www.nrc.gov/materials/fuel-cycle-fac/stages-fuel-cycle.html>.
16. R. J. Silva and H. Nitsche, *Radiochimica Acta*, 1995, **70/71**, 377-396.
17. Radioactive Waste, U.S. Nuclear Regulatory Commission, <https://www.nrc.gov/waste.html>.
18. G. F. de Melo and D. A. Dixon, *J Phys Chem A*, 2022, **126**, 6171-6184.
19. J. G. F. Romeu and D. A. Dixon, *J Phys Chem A*, 2025, **129**, 1396-1410.
20. G. F. de Melo and D. A. Dixon, *J Phys Chem A*, 2023, **127**, 3179-3189.
21. M. Vasiliu, K. A. Peterson, M. Marshall, Z. Zhu, B. A. Tufekci, K. H. Bowen and D. A. Dixon, *J Phys Chem A*, 2022, **126**, 198-210.
22. R. M. Cox, A. Kafle, P. B. Armentrout and K. A. Peterson, *J Chem Phys*, 2019, **151**, 034304.
23. G. F. de Melo, M. Vasiliu, M. Marshall, Z. Zhu, B. A. Tufekci, S. M. Ciborowski, M. Blankenhorn, R. M. Harris, K. H. Bowen and D. A. Dixon, *J Phys Chem A*, 2022, **126**, 4432-4443.
24. G. F. de Melo and D. A. Dixon, *J Phys Chem A*, 2023, **127**, 1588-1597.
25. G. F. de Melo, M. Vasiliu, G. Liu, S. Ciborowski, Z. Zhu, M. Blankenhorn, R. Harris, C. Martinez-Martinez, M. Dipalo, K. A. Peterson, K. H. Bowen and D. A. Dixon, *J Phys Chem A*, 2022, **126**, 9392-9407.



26. G. F. de Melo, M. Vasiliu, G. Liu, S. Ciborowski, Z. Zhu, M. Blankenhorn, R. Harris, C. Martinez-Martinez, M. Dipalo, K. A. Peterson, K. H. Bowen and D. A. Dixon, *J Phys Chem A*, 2022, **126**, 7944-7953.
27. J. G. F. Romeu, A. R. E. Hunt, G. F. de Melo, K. A. Peterson and D. A. Dixon, *J Phys Chem A*, 2024, **128**, 5586-5604.
28. B. A. Tufekci, K. Foreman, J. G. F. Romeu, D. A. Dixon, K. A. Peterson, L. Cheng and K. H. Bowen, *J Phys Chem Lett*, 2024, **15**, 11932-11938.
29. J. R. Schmitz and M. C. Heaven, *Journal of Molecular Spectroscopy*, 2021, **377**, 111426.
30. Occupational Safety and Health Administration, U.S. Department of Labor, Beryllium, <https://www.osha.gov/beryllium>, <https://www.osha.gov/beryllium>.
31. A. Kramida, Y. Ralchenko and J. Reader, *NIST Atomic Spectra Database (Version 5.3)*. National Institute of Standards and Technology, Gaithersburg, MD. 2015 <http://physics.nist.gov/asd>.
32. I. R. Ariyaratna and E. Miliordos, *J Phys Chem A*, 2017, **121**, 7051-7058.
33. I. R. Ariyaratna, S. N. Khan, F. Pawlowski, J. V. Ortiz and E. Miliordos, *J Phys Chem Lett*, 2018, **9**, 84-88.
34. I. R. Ariyaratna and E. Miliordos, *International Journal of Quantum Chemistry*, 2018, **118**.
35. A. Kalemios, I. R. Ariyaratna, S. N. Khan, E. Miliordos and A. Mavridis, *Computational and Theoretical Chemistry*, 2019, **1153**, 65-74.
36. I. R. Ariyaratna and E. Miliordos, *J Phys Chem A*, 2020, **124**, 9783-9792.
37. M. M. Montero-Campillo, O. Mó, M. Yáñez, I. Alkorta and J. Elguero, in *Advances in Inorganic Chemistry*, 2019, vol. 73, ch. 3, pp. 73-121.
38. D. R. Lide, *CRC Handbook of Chemistry and Physics*, 93rd ed., CRC press, New York, 2012.
39. H.-J. Werner and P. J. Knowles, *J. Chem. Phys.*, 1988, **89**, 5803-5814.
40. P. J. Knowles and H.-J. Werner, *Chem. Phys. Lett.*, 1988, **145**, 514-522.
41. K. R. Shamasundar, G. Knizia and H. J. Werner, *J. Chem. Phys.*, 2011, **135**, 054101.
42. K. Raghavachari, G. W. Trucks, J. A. Pople and M. Head-Gordon, *Chem. Phys. Lett.*, 1989, **157**, 479-483.
43. H. J. Werner, P. J. Knowles, G. Knizia, F. R. Manby and M. Schütz, *WIREs Comput. Mol. Sci.*, 2011, **2**, 242-253.
44. H. J. Werner, P. J. Knowles, F. R. Manby, J. A. Black, K. Doll, A. Hesselmann, D. Kats, A. Kohn, T. Korona, D. A. Kreplin, Q. Ma, T. F. Miller, 3rd, A. Mitrushchenkov, K. A. Peterson, I. Polyak, G. Rauhut and M. Sibaev, *J. Chem. Phys.*, 2020, **152**, 144107.
45. H.-J. Werner and P. J. Knowles, and others, *MOLPRO, version 2023.2, a package of ab initio programs*, <https://www.molpro.net>.
46. B. P. Prascher, D. E. Woon, K. A. Peterson, T. H. Dunning and A. K. Wilson, *Theoretical Chemistry Accounts*, 2011, **128**, 69-82.
47. K. A. Peterson, *J Chem Phys*, 2015, **142**, 074105.
48. R. Feng and K. A. Peterson, *J Chem Phys*, 2017, **147**, 084108.
49. A. Weigand, X. Cao, T. Hangele and M. Dolg, *J Phys Chem A*, 2014, **118**, 2519-2530.
50. H.-J. Werner and P. J. Knowles, *J. Chem. Phys.*, 1985, **82**, 5053-5063.
51. P. J. Knowles and H.-J. Werner, *Chem. Phys. Lett.*, 1985, **115**, 259-267.
52. D. A. Kreplin, P. J. Knowles and H. J. Werner, *J. Chem. Phys.*, 2019, **150**, 194106.
53. D. A. Kreplin, P. J. Knowles and H. J. Werner, *J. Chem. Phys.*, 2020, **152**, 074102.
54. S. R. Langhoff and E. R. Davidson, *International Journal of Quantum Chemistry*, 1974, **8**, 61-72.
55. F. N. N. Pansini, A. C. Neto and A. J. C. Varandas, *Theoretical Chemistry Accounts*, 2016, **135**, 261.
56. F. N. N. Pansini, A. C. Neto and A. J. C. Varandas, *Chemical Physics Letters*, 2015, **641**, 90-96.
57. M. Kallay, P. R. Nagy, D. Mester, Z. Rolik, G. Samu, J. Csontos, J. Csoka, P. B. Szabo, L. Gyevi-Nagy, B. Hegely, I. Ladjanszki, L. Szegedy, B. Ladoczki, K. Petrov, M. Farkas, P. D. Mezei and A. Ganyecz, *J Chem Phys*, 2020, **152**, 074107.



58. M. Kállay, P. R. Nagy, D. Mester, L. Gyevi-Nagy, J. Csóka, P. B. Szabó, Z. Rolik, G. Samu, J. Csontos, B. Hégyel, Á. Ganyecz, I. Ladjánszki, L. Szegedy, B. Ladóczki, K. Petrov, M. Farkas, P. D. Mezei and R. A. Horváth, *MRCC, A Quantum Chemical Program Suite. Budapest University of Technology and Economics, Budapest. www.mrcc.hu*.
59. E. D. Glendening, C. R. Landis and F. Weinhold, *J Comput Chem*, 2019, **40**, 2234-2241.
60. E. D. Glendening, J. K. Badenhoop, A. E. Reed, J. E. Carpenter, J. A. Bohmann, C. M. Morales, P. Karafiloglou, C. R. Landis and F. Weinhold, *Natural Bond Order 7.0; Theoretical Chemistry Institute, University of Wisconsin: Madison, WI*, 2021.
61. I. R. Ariyaratna, *Phys Chem Chem Phys*, 2025, **27**, 13183-13193.
62. R. Tang, R. Si, Z. Fei, X. Fu, Y. Lu, T. Brage, H. Liu, C. Chen and C. Ning, *Phys Rev Lett*, 2019, **123**, 203002.
63. Electronegativity in the Periodic Table of Elements. National Center for Biotechnology Information, 2024, <https://pubchem.ncbi.nlm.nih.gov/periodic-table/electronegativity>.
64. G. Knizia, *J Chem Theory Comput*, 2013, **9**, 4834-4843.
65. I. R. Ariyaratna and E. Miliordos, *J Quant Spectrosc Ra.*, 2020, **255**, 107265.
66. N. M. S. Almeida, I. R. Ariyaratna and E. Miliordos, *Phys Chem Chem Phys*, 2018, **20**, 14578-14586.
67. I. R. Ariyaratna, *Phys Chem Chem Phys*, 2024, **26**, 21099-21109.
68. I. R. Ariyaratna, J. A. Leiding, A. J. Neukirch and M. C. Zammit, *Phys Chem Chem Phys*, 2025, **27**, 1402-1414.
69. I. R. Ariyaratna, *Phys Chem Chem Phys*, 2024, **26**, 22858-22869.
70. J. D. Cox, D. D. Wagman and V. A. Medvedev, *CODATA Key Values for Thermodynamics*, Hemisphere Publishing Corp., New York, 1989.
71. D. D. Wagman, W. H. Evans, V. B. Parker, R. H. Schumm, I. Halow, S. M. Bailey, K. L. Churney and R. L. Nuttall, *J. Phys. Chem. Ref. Data* 1982, **11**, Suppl. 2.
72. L. A. Curtiss, K. Raghavachari, P. C. Redfern and J. A. Pople, *The Journal of Chemical Physics*, 1997, **106**, 1063-1079.



Data availability statement

The data supporting this article have been included as part of the Supplementary Information.

